An Ion Diffusion Method for Visualising a Solid-like Water Nanofilm

Ya Wang*, Zhiguang Duan* & Daidi Fan

Shaanxi Key Laboratory of Degradable Biomedical Materials, School of Chemical Engineering, Northwest University, Xi'an 710069, China.

Correspondence and requests for materials should be addressed to D.D.F. (fandaidi@nwu. edu.cn; lanmao1998@163. com)

* These authors contributed equally to this work.

A nano-thick solid-like water film on solid surfaces plays an important role in various fields, including biology, materials science, atmospheric chemistry, catalysis and astrophysics. Visualising the water nanofilm has been a challenge due to its dynamic nature and nanoscale thickness. Here we report an ion diffusion method to address this problem using a membrane formed with a BSA-Na_2CO_3 (BSA, bovine serum albumin) mixture. After a solid-like water nanofilm deposits onto the membrane, Na^+ and CO_3^{2-} ions diffuse into the film to form a solid Na_2CO_3 phase in its place. Consequently, the morphology of the nanofilm can be visualised by the space filled by the Na_2CO_3. Using this method, we successfully observed polygon-like, ribbon-like and spot-like nanofilms at 193 K, 253 K and room temperature, respectively. Our method may provide a tool for characterising confined water films ranging from a few nanometres to hundreds of nanometres in thickness.

A solid-like water film ubiquitously covers all surfaces not only at ultralow temperatures[1,2], but also at room temperature[3–5]. This film, which exhibits characteristics that differ from those of bulk water and give the substrate many important physical and chemical properties[6,7], plays an important role in diverse scientific fields. Over the past few decades, numerous methods have been employed to determine the thickness[3,8,9], structures[6,7,10–12] and thermodynamic properties[2,6,13] of the solid-like water film. Among these methods, scanning probe microscopy (SPM) seems to be the only approach capable of directly visualising the film. Although SPM has been used extensively to study the water film on solids and has expanded our understanding[3,5,8–11], serious technical challenges remain for its application because a solid-like water film often consists of two sublayers: a solid sublayer near the solid substrate and a semisolid sublayer near the vapour (see Supplementary Information section 1 for more details). Different from the solid sublayer, the semisolid sublayer is considered to be soft and dynamic, behaving much like liquid water[14]. Thus, when the SPM tip is applied close enough to the sample, capillary menisci that form between the tip and sample may strongly perturb the water film and confound the imaging. Additionally, the tip-sample interactions may induce a structural transition of the semisolid sublayer according to the study by Choi *et al*[15]. in which the tip induced a liquid-to-solid phase transition of water at room temperature.

Here we report for the first time the use of a BSA-Na_2CO_3 membrane as an imaging base (IB) to visualise the water nanofilm based on the diffusion of ions within the membrane. Previous studies have demonstrated that small molecules and ions are able to diffuse in a solid-like water film[16–18]. In this study, we demonstrated that the Na^+ and CO_3^{2-} ions diffused into the "solid-like" water film covering the IB surface, transforming the film to an actual "solid" Na_2CO_3 phase. The resulting morphology of the "solid" phase was treated as that of the water film and was reliably observed using an AFM (atomic force microscope) or SEM (scanning electron microscope).

Results

The imaging base (IB). The IB was a membrane formed from a BSA and Na_2CO_3 mixture in which Na_2CO_3 served as the source of ions (Na^+ and CO_3^{2-}) to fill the water nanofilm and BSA served as the skeleton to stabilise the overall shape of the membrane. As a polymer, BSA was chosen for the following reasons. First, BSA can be mixed with Na_2CO_3 to form a non-uniform membrane in which Na_2CO_3 is enriched on the top and bottom surfaces and BSA is enriched in the middle, forming a three-layer phase distribution called a sandwich structure (see Supplementary Information section 2 for more details). This structure is important for visualising the water nanofilm, which will be discussed in detail in the following sections. Second, BSA molecules are difficult to diffuse into the water nanofilm due to their large size and strong intermolecular interactions. Third, BSA does not react with Na_2CO_3. In our experiments, a mixture with an ultra-flat (nanometre-scale roughness) and amorphous top
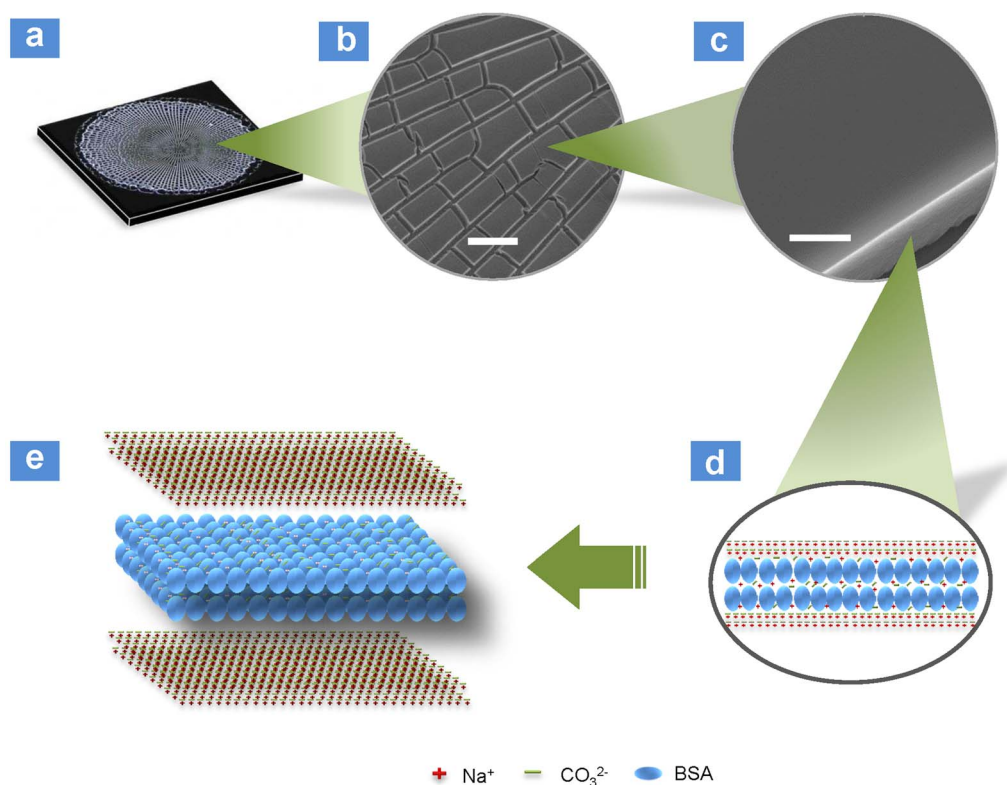
Figure 1 | The sandwich structure that serves as the imaging base (IB) for visualising the solid-like water film. (a), A general view of the IB (diameter of ~5–8 mm). (b), (c), SEM images of the IB. Scale bars for (b) and (c) are 100 μm and 5 μm, respectively. (d), (e), A model of the sandwich structure.

surface was employed to visualise the confined water nanofilm (Fig. 1 and Fig. S3). The surface of the mixture was featureless, which is favourable for the formation of a water nanofilm. XPS (X-ray photoelectron spectroscopy) images indicated that Na, C and O elements were uniformly distributed on the surface (Fig. S4), implying that the distribution of Na^+ and CO_3^{2-} ions should be uniform as well. This uniformity ensures that the ions from different areas of the surface have an equal likelihood of diffusing into the water film.

The sandwich structure plays an important role in visualising the water nanofilm. When a solid-like water film with rugged morphology is adhered to the IB surface, the outermost Na_2CO_3-rich phase guarantees that sufficient ions (Na^+ and CO_3^{2-}) diffuse into the water film to form a compact solid phase in place of the profile of the film itself (Fig. 2a). During this process, if the ions from the Na_2CO_3-rich phase are exhausted, the ions from the middle BSA-rich phase will serve as a backup source to maintain the continuity of the top-layer ions. Moreover, BSA enrichment in the middle layer guarantees the stability of the overall shape of the IB, as the ions constantly diffuse into the water film. Compared to the upper two layers, the bottom Na_2CO_3-rich phase is not as critical for visualising the nanofilm, but this phase is useful for evaluating the water vapour near the IB with the naked eye under different conditions. Generally, an increased amount of water vapour near the IB would reduce the transparency of the IB (see Supplementary Information section 4 for more details).
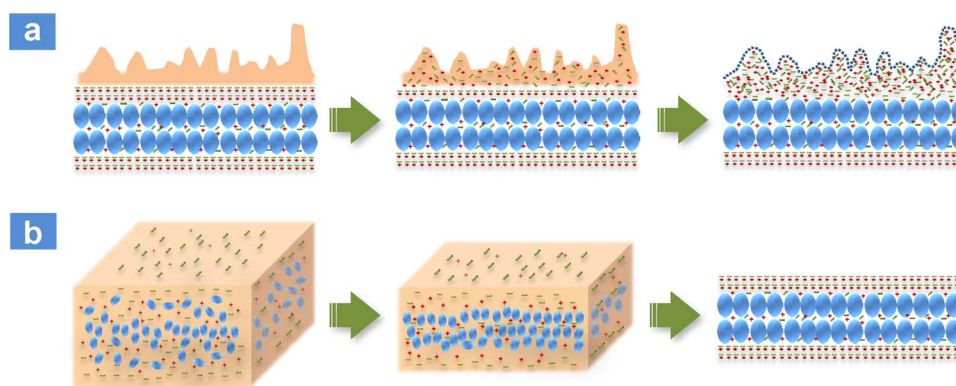

Figure 2 | The strategy for nanofilm visualisation and the formation process of the sandwich structure. (a), The strategy for nanofilm visualisation. A solid-like water film deposits onto the IB surface (left). Then, Na^+ and CO_3^{2-} ions diffuse into the film (middle) and eventually form a solid phase (right). (b), The formation process of the sandwich structure. BSA molecules are enriched in the middle layer of the liquid film as the water evaporates (left). Then, the BSA-rich phase becomes compact, and Na^+ and CO_3^{2-} ions are excluded from the BSA-rich layer to form the Na_2CO_3-rich layers (middle). The sandwich structure finally forms when the liquid film is dried fully (right).

In our studies, the formation of a sandwich-like structure was accomplished by a phase separation process. Briefly, a drop of BSA-Na$_2$CO$_3$ solution was added onto the substrate and then air-dried under ambient conditions. During this process, the polymer BSA underwent a transition called glassy-state structural relaxation in which the BSA was gradually concentrated as water evaporated, and the BSA transformed into a glassy-state (an amorphous and compact solid state)[19]. As the relaxation rate of the bulk solution was significantly faster than the air/water or water/substrate interfaces[19], BSA was first enriched in the middle phase and served as a scaffold for the entire mixture (see Supplementary Information section 5 for more details). With the loss of water, the middle phase became increasingly crowded, leading to an excluded volume effect[20]. This effect means that some ions (Na$^+$ and CO$_3^{2-}$), along with some water, were excluded from the BSA-rich domain to form a Na$_2$CO$_3$-rich phase on both sides of the BSA-rich phase (Fig. 2b). Additionally, the nanoparticle effect may be involved in this process. A BSA molecule can be considered an ellipsoidal nanoparticle because of its size ($14 \times 4 \times 4$ nm in dimension)[21]. The large surface area gives BSA molecules high surface energy, which makes them unstable and inclined to aggregate compactly, similar to the manner in which iron oxyhydroxide nanoparticles form compact crystals in a liquid cell[22]. The non-homogeneous ion distribution effect might also play a role in the formation process. Ion distribution at the air/water interface has been suggested to be non-homogeneous[23,24]. Compared with cations, anions are more likely to be located at the air-water interface[24]. Cations (Na$^+$) in water are bonded to the oxygen atoms in water so that the water molecules are distributed fairly symmetrically around the ion (Fig. S7, left). In contrast, large anions (CO$_3^{2-}$) bind to the hydrogen atoms in water to enable hydrogen bonding between the anion and water, leading to an asymmetrical arrangement of water molecules around the ion (Fig. S7, right). Accordingly, cations prefer the homogeneous environment in bulk water, whereas anions form asymmetric structures near the interface. Similarly, the non-homogeneous ion distribution should also exist at the solid-water interface. Therefore, the anions would be greatly enriched near the surfaces at the later stages of the drying process, attracting the cations to be enriched at the surfaces as well.

The water nanofilm at 193 K. Water molecules prefer to build hexagonal nanostructures[10,12] (Fig. S8) that then evolve into mesoscopic hexagonal ice flakes[25–27] (Fig. 3a) when the temperature drops below zero. We intended to capture these flakes with the IB to test the applicability of our method. Previous studies[26] have indicated that ice exhibits varying morphologies at different levels of supersaturation. When the supersaturation (at a certain temperature) is low
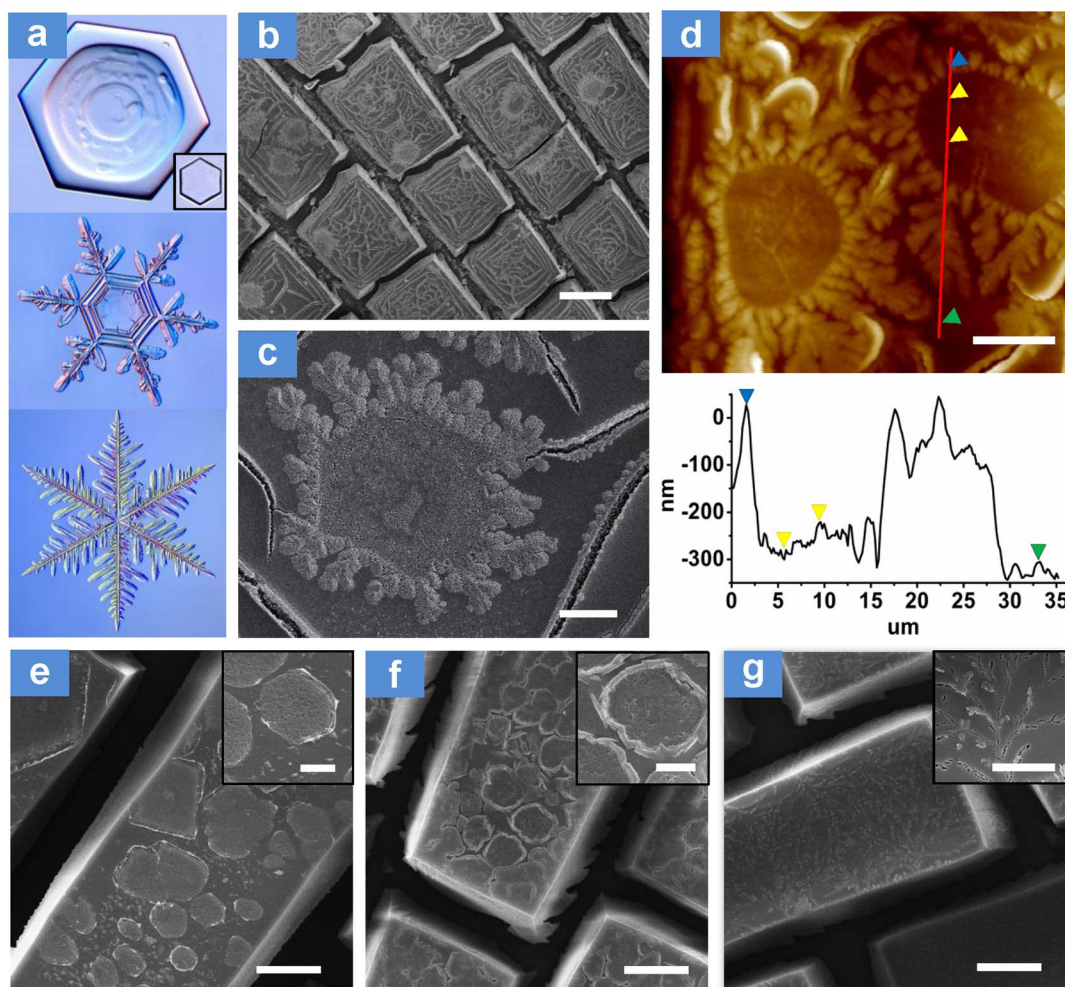
Figure 3 | Some typical morphologies of the solid-like films at 193 K. (a), Some regular ice flakes. Images reproduced from Ref. [27], with permission from Kenneth G. Libbrecht. (b) and (c), SEM and (d), AFM (contact mode) images obtained from an IB sealed at 193 K for 5 days. The height profile (bottom, (d)) is given for the red line. The height of the edge, inside and outside are marked with blue, yellow and green triangles, respectively. (e–g), SEM images of water nanofilms obtained under different conditions. The IB was unsealed at 193 K for 5 days (e), sealed at 193 K for 1–2 h and then unsealed for 3–4 h (f), or sealed at 193 K for 1–2 h and placed face down (default was face up) on the plate for 3–4 h (g). Scale bars: 40 μm, 5 μm and 10 μm for (b–d), respectively; 20 μm for (e–g); 5 μm for the insets in (e), (f) and (g).

enough, a flat hexagonal flake (inset, top panel in Fig. 3a) seems to form easily. As the supersaturation increases, hexagonal flakes with a bulging (top panel in Fig. 3a) or branching edge (middle panel in Fig. 3a) and tree-like flakes (bottom panel in Fig. 3a) are likely to appear. In our experiments, we focused on capturing the most common flake, i.e., the flake with a branching edge. Considering that such a flake usually occurs at relatively high supersaturation, the IB was sealed in a small plate at a RH (relative humidity) of 15–25% at room temperature, and a supersaturated environment was produced inside by placing the IB at 193 K for 4–6 days. Rapid cooling would quickly convert the sealed vapour into ice to limit the damage on the IB surface caused by liquid water. Then, the IB was freeze-dried under a low vacuum pressure (<100 mTorr) and observed using an SEM or AFM. Here the freeze-drying process was introduced to accelerate the diffusion rate of the ions. Under low vacuum pressure (lower than the triple-point of water), the confined water film was maintained in a solid-like state and firmly confined to the IB surface with limited sublimation[28]. As the temperature of the IB slowly rose by heat exchange with the ambient environment (room temperature), Na^+ and CO_3^{2-} ions diffused into the solid-like film with increasing speed until equilibrium was reached.

By SEM, the morphology of the resulting nanofilm was mostly a dendritic morphology, except for some scattered polygonal ice flakes with branching edges (Fig. 3b). A rare, well-defined hexagonal flake was shown in Fig. 3c, which was quite similar to that shown above (middle panel in Fig. 3a). The height of these flakes was measured using AFM (Fig. 3d). The flakes were ~350 nm high at the edge (marked with a blue triangle) relative to its outside base (marked with a green triangle), but the flakes were only ~10–100 nm high inside (marked with yellow triangles). According to Libbrecht, such an uneven height distribution of the flake might be caused by small bumps that appear on a flat flake surface at relatively high

supersaturation[27]. The bumps grew faster than the rest of the flake and developed into large branches on the flat flake as the water molecules in the vapour contacted the bump more quickly than other parts of the flake. In addition, some flakes with shapes similar to those mentioned above (shown in Fig. 3a) were also observed. The flat polygonal flakes (Fig. 3e) were formed at low supersaturation by directly exposing the IB at 193 K for a few days. Polygonal flakes with raised edges (Fig. 3f) were observed when the IB was sealed for 1–2 h and then exposed for 3–4 h at 193 K. Tree-like flakes (Fig. 3g) were observed when the IB was sealed for 1–2 h at 193 K and then placed face down on the plate (default was 'face up') for 3–4 h. In conclusion, all the above observations at 193 K showed great potential for visualising the solid-like water nanofilm using the IB.

The water nanofilm at room temperature. The solid-like film not only exists at ultralow temperatures but also at room temperature. Studies have indicated that all hydrophilic surfaces are coated with a nanometre-scale (one to a few water monolayers in thickness) ice-like film at room temperature[3–5]. Because a few dangling OH bonds exist in the ice-like layer, a nanoscale water droplet cannot completely wet this layer and hence forms nanoscale spot-like bulges[28,29] (Fig. 4a). A similar result was observed in our experiments when the IB was sealed at a low RH (15–25%) at room temperature for 3–5 days. The surface of the IB was covered with many amorphous bulges (average lateral size >100 nm), which were ~3–5 nm above the initial surface (Fig. 4b and Supplementary Information section 8). These bulges were amorphous and loosely embedded on the surface, implying that the droplet was not liquid (the ions in a liquid should grow into crystals). Therefore, we believe that the droplet and the ultrathin water layer underneath it have roles in the semisolid sublayer and solid sublayer, respectively. When the IB was processed at a lower humidity (<10% RH), the surface remained
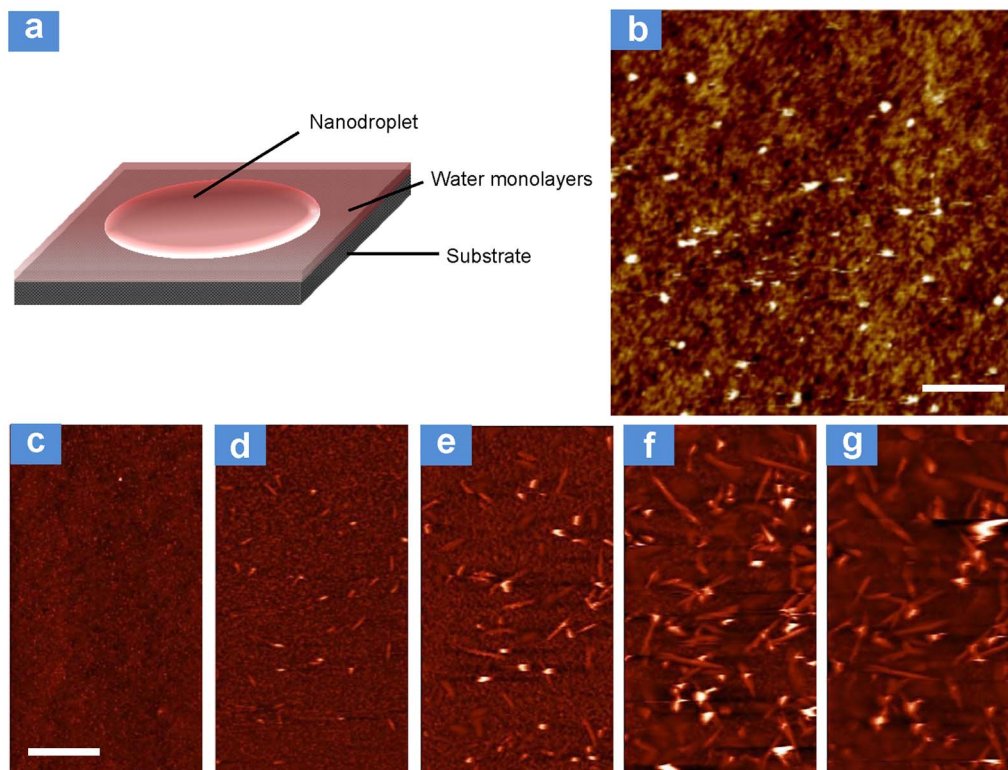
Figure 4 | The solid-like water films at room temperature. (a), A proposed model of a solid-like water film at room temperature. (b), AFM image (contact mode) of an IB placed at room temperature (15–25% RH) for 3–5 days. (c–g), AFM images (semi-contact mode) for the dynamic process of Na_2CO_3 self-assembly in a water nanofilm at room temperature. These images were captured within 40 min after the IB was transferred to room temperature (~50–55% RH). Scale bars: 1 μm for (b) and 2 μm for (c–g).
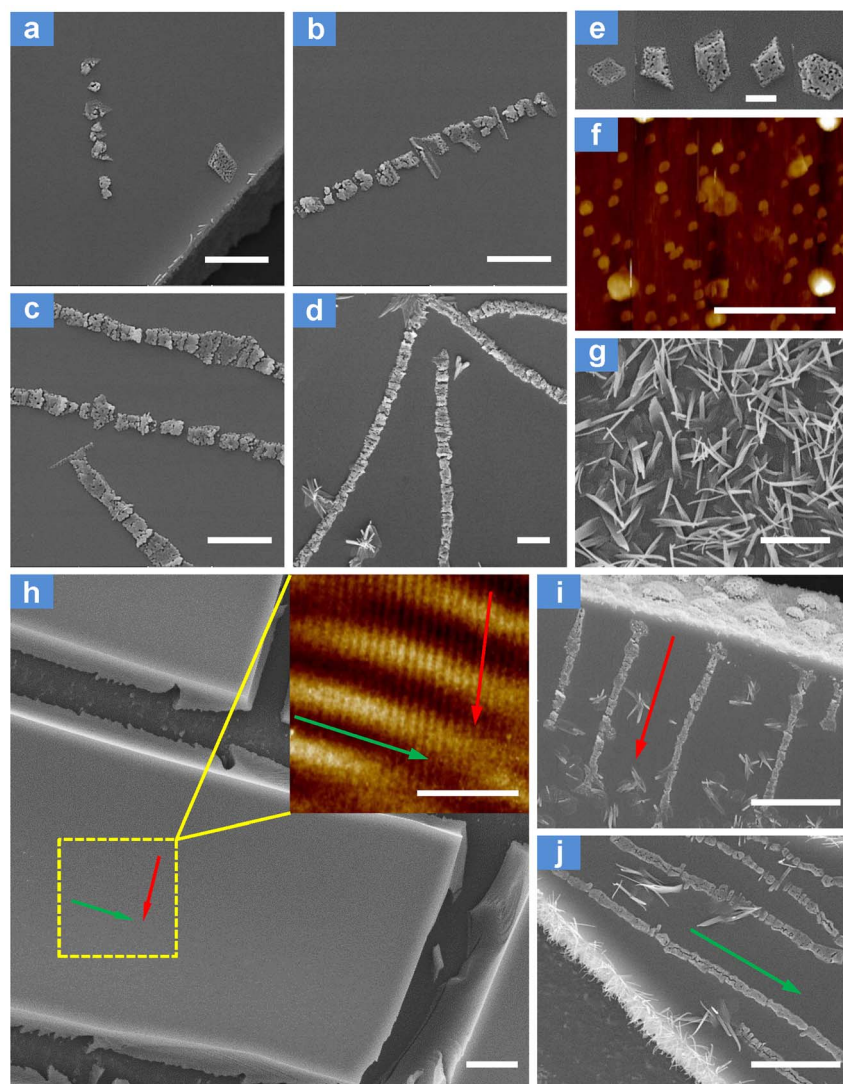
Figure 5 | The morphologies of solid-like films at 253 K. (a–e), (i), (j), SEM images obtained from an IB sealed at 253 K for 3–5 days. (e) represents a composite picture of several images captured at different positions to show individual polygon-like bulges. The direction of the ribbons in (i) and (j) is indicated by green and red arrows, respectively. (f), AFM image of an IB sealed at 253 K for 12 h. (g), SEM image of an IB sealed at 253 K for 7 days. (h), A high-resolution SEM image and AFM image (inset) of the troughs on the IB surface. Directions of the troughs parallel to the IB fragment and the ones perpendicular to the IB fragment are indicated by green and red arrows, respectively. Scale bars: 5 μm for (a–d), (g) and inset in (h); 2 μm for (e) and (f); 10 μm for (h–j).

unchanged even after a longer time (Fig. S9b), which implies that the bulges were caused by the water nanodroplets. On the other hand, when the IB was processed at high humidity (50–55% RH), the IB was quickly covered with needle-like Na_2CO_3 crystals, which seemed to appear suddenly and then grew in number and size at a fixed location (Fig. 4c–g). We think that the water film in this case is flat and more liquid-like, but still not liquid. A liquid water film tends to cause dissolution damage on the surface (BSA and Na_2CO_3 are water-soluble) and seems unfavourable for a nanoparticle to grow or stay in the same location.

To conclude the above results, we developed a hypothesis to describe the dynamic behaviours of the water nanofilm under different RH conditions at room temperature. When the IB is exposed to quite low RH conditions, the surface is covered with an ultra-thin water film that consists of only a few water monolayers. The film is so thin and evenly distributed on the surface that it has no clear effects on the morphology of the IB. As RH increases, more water vapour condenses onto the film, forming semi-solid nanodroplets in which the ions are only allowed to form an amorphous-state solid by diffusion. When the RH reaches a certain level, the droplets increase in number and fully cover the surface, forming a flat and more liquid-like nanofilm in which both diffusion and self-assembly allow the formation of crystals. Finally, the water nanofilm eventually becomes a liquid film when the RH reaches oversaturation.

The water nanofilm at 253 K. The above-mentioned water nanofilms at 193 K and room temperature are relatively easy to understand. In some other cases, however, the film presents unreported morphologies. Here we used a water nanofilm at 253 K as an example to show some unusual morphologies. The IB sealed at 15–25% RH (room temperature) was placed at 253 K for 3–5 days and then observed at room temperature. The resulting surface was often covered with many micrometre-size amorphous 'ribbons' (Fig. 5a–e) that were built from polygonal flakes and usually had a height of dozens of nanometres to hundreds of nanometres over the surface. Meanwhile, some single flakes of quadrangular or pentagonal shape were also captured (Fig. 5e). We gathered many images and rearranged their sequence (Fig. 5, a → d) to establish the process by which single polygonal flakes evolve into ribbons. At the initial stage, the water vapour deposited onto the IB and gradually formed a number of polygon-like bulges

(Fig. 5e). These bulges tended to be aligned discretely instead of being interconnected (Fig. 5a). Subsequently, more bulges formed in the same manner and formed longer fragments (Fig. 5b,c) that were finally interconnected and developed into continuous ribbons (Fig. 5d). The ribbon-like morphology was only present at a specific processing time at 253 K. When the processing time was too short (≤12 h), not enough vapour seemed to deposit onto the IB, which resulted in a spot-like morphology (Fig. 5f) similar to that observed at room temperature and as shown in Figure 4b, except the spots were larger and more compact. If the processing time was too long (≥7 days), the water film seemed to become more liquid-like and induced the ions to self-assemble into regular needle-like crystals (Fig. 5g), similar to that observed at room temperature and as shown in Fig. 4g. We also noted that many needle-like crystals sprouted from the ribbons (Fig. 5d). These results strongly supported the notion that the ribbon-like morphology served as a transition state from a spot-like to needle-like morphology.

Carrasco and coworkers[11] found that one-dimensional (1D) water chains (with a period of 7.2 Å and lateral separation of 5.4 Å) sat steadily in the troughs between the Cu rows at low coverage, implying that the 1D hydrogen bond arrangement might be formed preferentially with minimal strain within the overlayer due to the existence of the periodical troughs. Similarly, we observed multiple areas of the IB surface and found some troughs (typically <3 μm in width and <7 nm in depth) in two directions: parallel or perpendicular to the IB fragment direction (indicated by green and red arrows, respectively, in Fig. 5h). Coincidentally, some ribbons aligned in a similar direction to the troughs were captured (Fig. 5i,j). Therefore, we postulated that the troughs might induce the alignment of the water precursors (Fig. 5e,f) to minimise the strain within the water overlayer and result in the ribbon-like fragments. Nevertheless, the behaviours of water at 253 K require further investigation.

Discussion

According to our data, the physical state of the water nanofilm appears quite sensitive to fluctuations in ambient conditions. In many cases, for example at 253 K, no clear boundary exists between the "more solid-like" and "more liquid-like" states. Therefore, characterising the film with the traditional SPM imaging method described at the beginning of the text is difficult. Our ion diffusion method provides a new way to explore the mysteries of the confined water film.

Methods

Preparation of the IB. A certain volume (~10–20 μl) of a mixed solution [75 mg ml⁻¹ BSA (low heavy metals; purity by SDS-PAGE, >98%; Merck), 15 mg ml⁻¹ Na$_2$CO$_3$ (purity, >99.8%; Rgent)] was added to the substrate (glass slide or silicon wafer) and dried for 4 h at 323–333 K in an oven (<8% RH).

Preparation of the water nanofilms. To obtain a water nanofilm, the IB was sealed in a plate (~7 cm in diameter and ~1.5 cm thick, Aicor) at low RH (~15–25%) at room temperature, allowing a small amount of water vapour inside (this procedure also guarantees that all samples are under the same amount of vapour in the environment). For the film at 193 K, the plate was processed in an ultralow temperature freezer (DW-86L386, Haier) for a specified time and then freeze-dried in the freeze dryer (FD5-10, SIM) for approximately 48 h. For the films at room temperature and 253 K, the plates were placed in the freezer (BCD-539wt, Haier) and at room temperature, respectively, for a specified time.

SEM and AFM observation. All samples were observed under natural RH conditions at room temperature. Generally, the samples were first observed with AFM then coated with an Au layer for SEM observation. Many samples were evaluated multiple times by different SEM instruments (Vega3, Tescan; G2 Pro, Phenom; SU8010, Hitachi) and AFM instruments (Solver Next, NT-MDT; Innova, Bruker) to ensure the reliability of the results.

XPS analysis. The IB was prepared and quickly analysed (time lag <1 min) by XPS (ESCALAB 250Xi, Thermo Fisher) to avoid diffusion of the ions into a newly formed water layer during the sample transfer process. To obtain reliable results, the IB surface was usually etched by an argon ion beam at 2–3 keV for 15–30 s to generate a fresh surface for element analysis.

Regarding RH control. All experiments were conducted under natural RH conditions rather than in a traditional CHC (controlled humidity chamber). RH control is usually difficult because RH fluctuation is sensitive and significant.

Moreover, it often takes a long time to reach equilibrium once the parameter changes. For example, the IB is intended to be observed at a target RH of 30% with CHC-equipped AFM, while the RH in ambient conditions is 50%. When the sample is transferred from ambient conditions (50%) to a CHC (30%), the CHC chamber must be opened, which causes a significant fluctuation in RH inside. Then, a long time lag is needed for the RH to return to 30%, during which time the IB surface may be changed by the unknown amount of water vapour. In contrast, the RH is much more stable under natural ambient conditions for this experiment.

1. Kaya, S., Weissenrieder, J., Stacchiola, D., Shaikhutdinov, S. & Freund, H.-J. Formation of an ordered ice layer on a thin silica film. *J. Phys. Chem. C.* **111**, 759–764 (2007).
2. Mitlin, S. & Leung, K. Film growth of ice by vapor deposition at 128–185 K studied by Fourier transform infrared reflection-absorption spectroscopy: Evolution of the OH stretch and the dangling bond with film thickness. *J. Phys. Chem. B.* **106**, 6234–6247 (2002).
3. Spagnoli, C., Loos, K., Ulman, A. & Cowman, M. K. Imaging Structured Water and Bound Polysaccharide on Mica Surface at Ambient Temperature. *J. Am. Chem. Soc.* **125**, 7124–7128 (2003).
4. Xu, K., Cao, P. & Heath, J. R. Graphene visualizes the first water adlayers on mica at ambient conditions. *Science* **329**, 1188–1191 (2010).
5. Teschke, O. Imaging Ice-Like Structures Formed on HOPG at Room Temperature. *Langmuir* **26**, 16986–16990 (2010).
6. Ewing, G. E. Thin Film Water. *J. Phys. Chem. B.* **108**, 15953–15961 (2004).
7. Ewing, G. E. Ambient Thin Film Water on Insulator Surfaces. *Chem. Rev.* **106**, 1511–1526 (2006).
8. Bluhm, H. & Salmeron, M. Growth of nanometer thin ice films from water vapor studied using scanning polarization force microscopy. *J. Chem. Phys.* **111**, 6947 (1999).
9. Döppenschmidt, A. & Butt, H.-J. Measuring the thickness of the liquid-like layer on ice surfaces with atomic force microscopy. *Langmuir* **16**, 6709–6714 (2000).
10. Michaelides, A. & Morgenstern, K. Ice nanoclusters at hydrophobic metal surfaces. *Nat. Mater.* **6**, 597–601 (2007).
11. Carrasco, J. *et al.* A one-dimensional ice structure built from pentagons. *Nat. Mater.* **8**, 427–431 (2009).
12. Feibelman, P. J. Partial dissociation of water on Ru (0001). *Science* **295**, 99–102 (2002).
13. Bolina, A. S., Wolff, A. J. & Brown, W. A. Reflection absorption infrared spectroscopy and temperature-programmed desorption studies of the adsorption and desorption of amorphous and crystalline water on a graphite surface. *J. Phys. Chem. B.* **109**, 16836–16845 (2005).
14. Li, Y. & Somorjai, G. A. Surface premelting of ice. *J. Phys. Chem. C.* **111**, 9631–9637.
15. Choi, E.-M., Yoon, Y.-H., Lee, S. & Kang, H. Freezing transition of interfacial water at room temperature under electric fields. *Phys. Rev. Lett.* **95**, 85701 (2005).
16. Li, H. *et al.* Peptide Diffusion and Self-Assembly in Ambient Water Nanofilm on Mica Surface. *J. Phys. Chem. B.* **113**, 8795–8799 (2009).
17. Ye, M., Zhang, Y., Li, H., Xie, M. & Hu, J. Supramolecular Structures of Amyloid-Related Peptides in an Ambient Water Nanofilm. *J. Phys. Chem. B.* **114**, 15759–15765 (2010).
18. Kim, J. H., Shin, T., Jung, K. H. & Kang, H. Direct observation of segregation of sodium and chloride ions at an ice surface. *ChemPhysChem* **6**, 440–444 (2005).
19. Priestley, R. D., Ellison, C. J., Broadbelt, L. J. & Torkelson, J. M. Structural Relaxation of Polymer Glasses at Surfaces, Interfaces, and In Between. *Science* **309**, 456–459 (2005).
20. Minton, A. P. The influence of macromolecular crowding and macromolecular confinement on biochemical reactions in physiological media. *J. Biol. Chem.* **276**, 10577–10580 (2001).
21. Peters Jr, T. *All about Albumin: Biochemistry, Genetics, and Medical Applications* (Academic Press, San Diego, 1996).
22. Li, D. *et al.* Direction-Specific Interactions Control Crystal Growth by Oriented Attachment. *Science* **336**, 1014–1018 (2012).
23. Jungwirth, P. & Tobias, D. J. Ions at the air/water interface. *J. Phys. Chem. B.* **106**, 6361–6373 (2002).
24. Garrett, B. C. Ions at the Air/Water Interface. *Science* **303**, 1146–1147 (2004).
25. Emoto, M. *The Hidden Messages in Water* (Atria Books, New York, 2005).
26. Libbrecht, K. G. The physics of snow crystals. *Rep. Prog. Phys.* **68**, 855 (2005).
27. Libbrecht, K. G. *SnowCrystals.com.* Available at: http://www.its.caltech.edu/~atomic/snowcrystals/ (Accessed: 1st Nov 2013).
28. James, M. *et al.* Nanoscale condensation of water on self-assembled monolayers. *Soft Matter* **7**, 5309–5318 (2011).
29. Wang, C. *et al.* Stable liquid water droplet on a water monolayer formed at room temperature on ionic model substrates. *Phys. Rev. Lett.* **103**, 137801 (2009).

Author contributions

D.F. and Y.W. conceived the project; Y.W. and Z.D. performed all the experiments and wrote the manuscript.

Additional information